Journal of Materials Chemistry C

PAPER

View Article Online
View Journal | View Issue

Cite this: J. Mater. Chem. C, 2015, 3, 9154

Optoelectronic characteristics of a near infrared light photodetector based on a topological insulator Sb_2Te_3 film

Kun Zheng,[a] Lin-Bao Luo,*[a] Teng-Fei Zhang,[a] Yu-Hung Liu,[bc] Yong-Qiang Yu,[a] Rui Lu,[a] Huai-Li Qiu,[b] Zhong-Jun Li[b] and J. C. Andrew Huang*[bc]

Received 15th June 2015,
Accepted 4th August 2015

DOI: 10.1039/c5tc01772f

www.rsc.org/MaterialsC

In this study, we present a near infrared (NIR) light photodetector based on a topological insulator antimony telluride (Sb_2Te_3) film, which was grown on sapphire by molecular beam epitaxy (MBE). Electrical analysis reveals that the resistance of the topological insulator decreases with increasing temperature in the temperature range of 8.5–300 K. Further optoelectronic characterization showed that the as-fabricated photodetector exhibits obvious sensitivity to 980 nm light illumination. The responsivity, photoconductive gain and detectivity were estimated to be 21.7 A/W, 27.4 and 1.22×10^{11} Jones, respectively, which are much better than those of other topological insulators based devices. This study suggests that the present NIR photodetector may have potential application in future optoelectronic devices.

Introduction

Topological insulators (*e.g.*, Bi_2Se_3,[1] Bi_2Te_3,[2] and Sb_2Te_3[3]) are bulk insulators with metallic surfaces. They are a kind of material characterized by a bulk band inversion and strong spin–orbit interaction which lead to surface states that bridge the bulk band gap. In the past decade, topological insulators have received substantial research attention owing to their exotic properties, and to date a number of synthetic methods such as pulsed-laser deposition (PLD),[4] chemical vapor deposition (CVD),[5] metal organic chemical vapor deposition (MOCVD),[6] and molecular beam epitaxy (MBE) have been developed to synthesize various topological insulator materials.[7,8] It is reported that due to the spin–orbit coupling and time-reversal symmetry,[2,5,9] there is low energy dissipation for the carriers on the surface states of topological insulators.[10,11] In addition, angle-resolved photoemission spectroscopy (ARPES) analysis has showed that the surface states are composed of an odd number of Dirac cones with helical spin-momentum textures.[12,13] Topological insulators have exhibited great potential in a number of applications including quantum computing,[14,15] spintronics,[16] thermoelectric devices,[4] photodetectors,[17–19] and superconductors.[20]

Of these devices with different functions photodetectors have received special research interest due to their wide-ranging applications in many areas such as light vision, military surveillance, and target detection.[21,22] For example, Zhang *et al.* have reported a new photodetector based on a polycrystalline topological insulator Bi_2Te_3 film.[23] They found that the as-fabricated device exhibited obvious sensitivity to both visible and near infrared light (NIR) illumination with excellent reproducibility and stability. The responsivity and gain were estimated to be 3.3×10^{-5} A W^{-1} and 3.85×10^{-5}, respectively. Moreover, Bao *et al.* employed a graphene–Bi_2Te_3 nano-heterojunction to fabricate photo-switches for detection of irradiation in the range 532–1550 nm. It was observed that the device had a very high responsivity of 10 A W^{-1}, and a photoconductive gain of 11.[24] Herein, we present a NIR photodetector based on a topological insulator Sb_2Te_3 film grown by MBE. It was found that the NIR photodetector exhibits obvious sensitivity to 980 nm light illumination at low temperature with excellent reproducibility. The responsivity, photoconductivity gain, and I_{on}/I_{off} were estimated to be 21.7 A W^{-1}, 27.4 and 2.36, respectively, which are much better than that of other topological insulator film based devices. This study suggests that the topological insulator Sb_2Te_3 film has great potential for future optoelectronic device applications.

Results and discussion

Fig. 1(a) schematically illustrates the device geometry of the as-fabricated NIR photodetector, which is fabricated from the topological insulator Sb_2Te_3 film with a thickness of ~50 nm.

[a] School of Electronic Science and Applied Physics and Anhui Provincial Key Laboratory of Advanced Materials and Devices, Hefei University of Technology, Hefei, Anhui 230009, P. R. China. E-mail: luolb@hfut.edu.cn
[b] Department of Physics, National Cheng Kung University, Tainan 701, Taiwan. E-mail: jcahuang@mail.ncku.edu.tw
[c] Taiwan Consortium of Emergent Crystalline Materials, Ministry of Science and Technology, Taipei 106, Taiwan

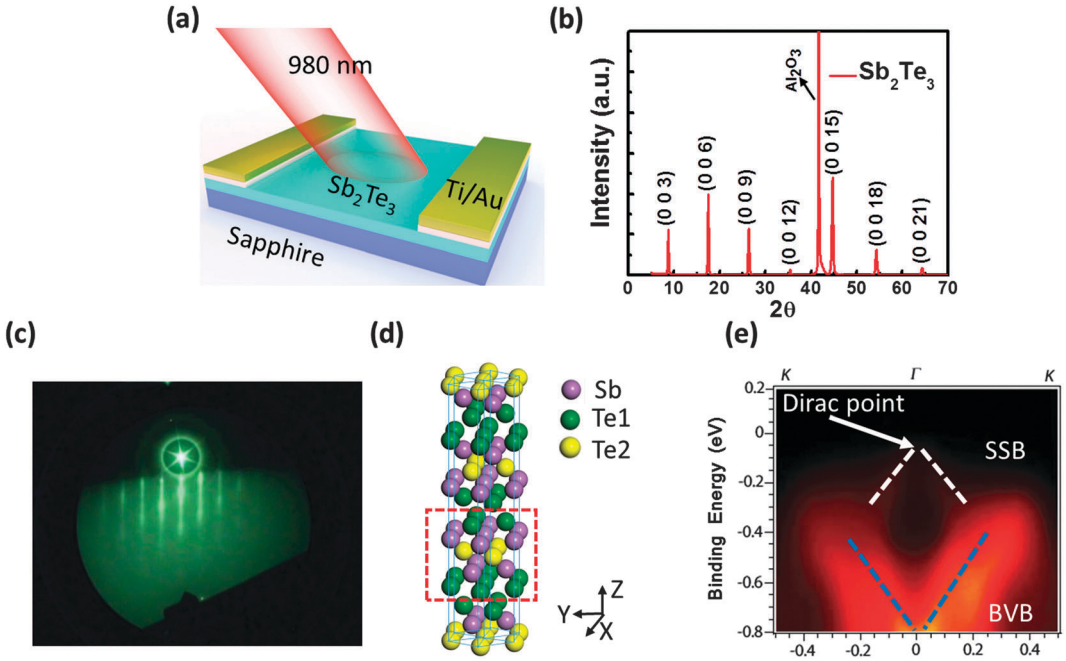

Fig. 1 (a) The schematic illustration of the NIR photodetector based on the topological insulator Sb_2Te_3 film. (b) The X-ray diffraction (XRD) pattern of the Sb_2Te_3 film grown at 250 °C by MBE. (c) The RHEED pattern of the Sb_2Te_3 film. (d) A schematic illustration of the crystal structure of the Sb_2Te_3 film. (e) The ARPES intensity map as a function of the binding energy and momentum.

From the XRD pattern of the film shown in Fig. 1(b), one can see clearly that all the diffraction peaks can be readily indexed to a rhombohedral crystal structure with a space group number of $R\bar{3}m$(166) (JCPDS Card No. 71-0393), consistent with the literature value.[25] In addition, the growth orientation is along the [00*X*] direction. The sharp streaky patterns of RHEED in Fig. 1(c) indicate that the topological insulator Sb_2Te_3 is of single crystal, which is different from the polycrystallinity of the topological insulator synthesized by PLD.[23] According to the schematic illustration shown in Fig. 1(d), the crystal structure of Sb_2Te_3 actually consists of five-atom layers along the *Z*-direction, which are known as quintuple layers. Each quintuple layer consists of five atoms with Te1–Sb–Te2–Sb′–Te1′ (Te1 and Te1′ and Sb and Sb′ are in equilibrium, Te2 is the third atom). The ARPES measurement along the *Γ*–*K* direction was then carried out to study the electronic band structure of the Sb_2Te_3 film. As shown in Fig. 1(e), the white lines show the upper surface state band (SSB), and the blue lines correspond to the bulk valence band (BVB). As a matter of fact, the topological insulator behavior of the Sb_2Te_3 film was also confirmed by the Dirac point slightly near the Fermi level around the *Γ* axis, which is consistent with theoretical calculations.[26]

The temperature-dependent current–voltage (*I*–*V*) curves of the topological insulator Sb_2Te_3 film was then studied in order to reveal its electrical characteristics. Fig. 2(a) and (b) compare the *I*–*V* characteristics at various temperatures ranging from 8.5 to 300 K in the dark and under 980 nm light illumination (6.2 mW cm^{-2}). It is clear that the resistance in the dark increases with decreasing temperature, which is attributed to the special electronic structure where the Fermi level is located near the Dirac point. The *I*–*V* curves in the dark exhibits a weak non-linear behavior, which is due to the existence of a barrier between the topological thin film and metal electrode. Interestingly, when illuminated by 980 nm light, the *I*–*V* curves are virtually linear, signifying that a good contact (Ohmic contact) was formed between the topological insulator film and Ti/Au electrode. It is also found that the dark-current increases with increasing temperature, in rough agreement with a previous study.[27] In fact, a similar phenomenon is also observed when the device is illuminated by 980 nm light. Notably, the currents under light illumination are all larger than that without illumination in the whole temperature region. From the temperature dependent resistances of the material at a bias of $V = 1$ V shown in Fig. 2(c), one can see that the resistance in the dark decreases more quickly than that under 980 nm light illumination. To estimate the contact resistance, we compared the *I*–*V* characteristic at temperatures of 45 and 300 K using both two- and four-probe methods [Fig. 2(d)]. The contact resistance between the Sb_2Te_3 film and Ti/Au electrode and the resistance of the Sb_2Te_3 film were estimated using the formula $2R_c + R_{4p} = R_{2p}$, where R_c is resistance of the contact resistance, R_{2p} and R_{4p} are the resistances measured by the two-probe and four-probe measurements, respectively. By fitting the linear part from −0.1 to 0.1 V, both the R_{2p} and R_{4p} at 45 K were calculated to be about 515.7 and 508.3 V, respectively. In addition, the contact resistance at this temperature is about 7.4, which is 1.46% of the resistance of the Sb_2Te_3 film. In addition, the contact resistance at 300 K is only 0.27% of the resistance of the Sb_2Te_3 film. In light of the relatively small contact resistance, we used a two-probe method in the optoelectronic measurements for convenience.

Considering the temperature-dependent electrical properties of the Sb_2Te_3 film, the photoresponse characteristics at different temperatures were then studied. As depicted in Fig. 3(a), the electrical

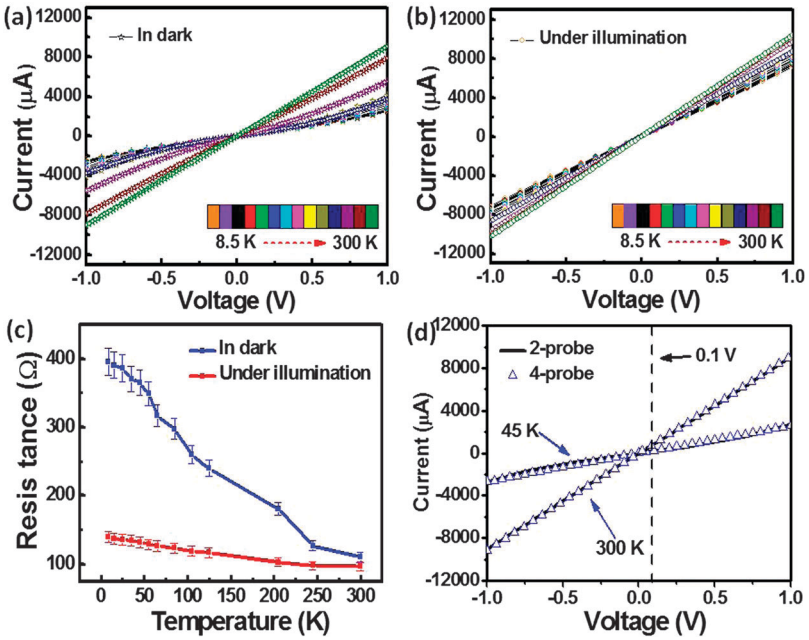

Fig. 2 Typical I–V curves of the Sb_2Te_3 film in the dark (a) and under illumination (b) at various temperatures from 8.5 to 300 K. (c) The comparison of the resistances in the dark and under 980 nm light illumination at different temperatures; the bias voltage is set to be 1 V. (d) The I–V characteristics of the Sb_2Te_3 film obtained by two- and four-probe measurements.

current increases to a high-conduction "on" state when irradiated by 980 nm light, but it decreases to low-conductivity "off" state after the NIR illumination was switched off. Unlike the conventional photodetectors based on semiconductor nanostructures with a very fast response speed,[28,29] the present device has a relatively slow rise time and fall time (~several hundred seconds). Such a difference in the response speed is probably due to their distinction in the working mechanism. In order to quantitatively evaluate the device performance of the NIR photodetector, the responsivity (R) and photoconductive gain (G) of the device at different temperatures are calculated using the following formulas:[30,31]

$$R = \frac{I_p - I_d}{P_{opt}} = \frac{\Delta I}{P_{opt}} = \eta\left(\frac{q\lambda}{hc}\right)G \quad (1)$$

$$G = R\frac{hc}{\eta q\lambda} \quad (2)$$

where I_p, I_d, P_{opt}, η, q, λ, h and c are the photocurrent, the current without light illuminated on, the power of the light which is irradiated on the device, the quantum efficiency (for convenience, assuming η = 1),[32] the absolute value of electron charge (1.6×10^{-19} Coulombs), the wavelength of illuminated light (980 nm), the Planck's constant (6.626×10^{-34} J s) and the velocity of light (3×10^8 m s^{-1}), respectively. Based on the above equations, the responsivity of the device at temperatures from 8.5 to 165 K keeps increasing until the maximum value of 3.5 A W^{-1} is reached. Then, the responsivity begins to decrease until 0.5 A W^{-1} in the temperature range from 165 to 300 K. A similar gain dependence on temperature was observed, as illustrated by the red curve in Fig. 3(b). The relatively high responsivity and gain at 150 K is related to the operation mechanism. As discussed later, the photocurrent of the present NIR photodetector was contributed by both the bulk and surface states, which exhibit different temperature dependent responsive

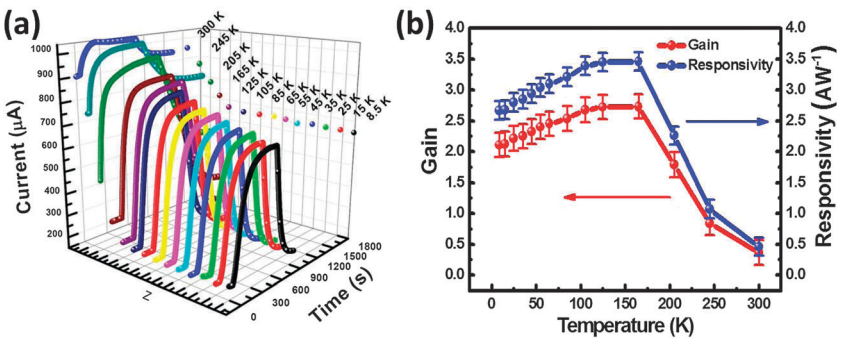

Fig. 3 (a) Time response of the topological insulator Sb_2Te_3 film photodetector under 980 nm light irradiation at different temperatures and a fixed bias of 0.1 V. (b) Responsivity and gain of the photodetector as a function of temperature.

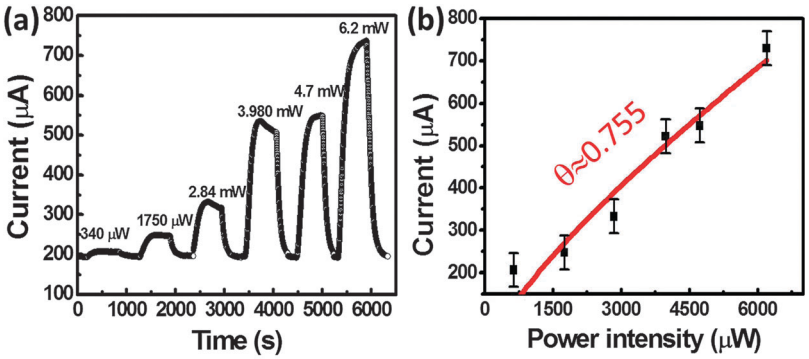

Fig. 4 (a) The photocurrent of the device with 980 nm light illuminated with different power intensities from 86.5 μW cm^{-2} to 6.2 mW cm^{-2}. (b) The relationship between the power intensity and the photocurrent.

behaviors: the bulk state (E_g: 0.26 eV), like other semiconductor materials, normally exhibits a high responsivity at room temperature, while the surface state in contrast is good at detecting at low temperature. Such a difference in optoelectronic properties causes a relatively high responsivity and gain at moderate temperature.

It is interesting to note that the photocurrent of the present NIR photodetector exhibits high dependence on the intensity of the incident irradiation as well. Fig. 4(a) plots the photocurrent of the Sb_2Te_3 photodetector under illumination with different power intensities ranging from 340 μW cm^{-2} to 6.2 mW cm^{-2}. It is clear that the photocurrent of the device increases gradually with increasing light intensity. Further quantitative analysis of the relationship between the photocurrent and the light intensity showed that the photocurrent can be fitted by a simple power law: $I = AP^{\theta}$, where A is the constant for a certain wavelength, P is the varied intensity of the light which is illuminated on the device and θ is a constant that determines the photosensitivity of the photodetector.[33] Fitting the equation by the experimental data gives $\theta \approx 0.755$ (Fig. 4(b)). It is clear that such a non-integer exponent can be regarded as a consequence of a complex process of electron–hole generation, trapping and recombination with the topological insulator film upon NIR irradiation.[31]

In addition to light intensity, the photocurrent of our topological insulator device is dependent on the bias voltage as well. Fig. 5(a) plots the dark current, photocurrent and on/off ratio (I_{on}/I_{off}) as a function of different bias voltages, from which the currents in the dark and under irradiation are observed to increase with increasing voltage at different rates, giving rise to a slow decrease with increasing bias voltage. To further reveal the bias voltage-dependent optoelectronic properties of the NIR photodetector, the photoresponse at bias voltages of 1, 0.1 and 0.01 V under NIR illumination that was periodically switched on and off is investigated. As shown in Fig. 5(b), at all 3 bias voltages, the present device displays obvious sensitivity to

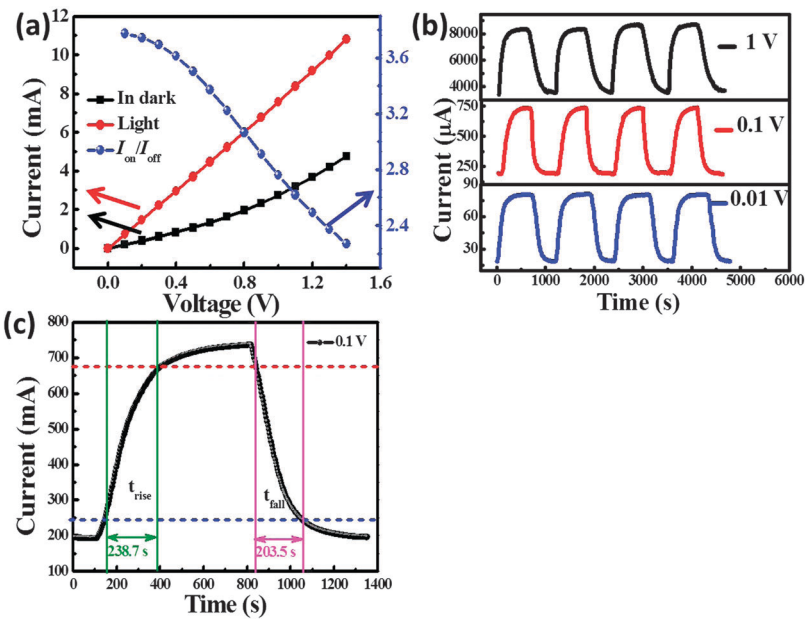

Fig. 5 (a) Dark current and photocurrent at a temperature of 45 K; the blue curve represents the on/off ratio. (b) Photoresponse of the photodetector based on the topological insulator Sb_2Te_3 at 45 K at different bias voltages V = 0.01 V, 0.1 V, 1 V. (c) One cycle of the photoresponse at a temperature of 45 K and a bias voltage of 0.1 V.

Table 1 Comparison of the device performance of the present photodetector and other topological insulator based photodetectors

	Wavelength (nm)	R (A W^{-1})	I_{light}/I_{dark}	G	D^* (Jones)	Ref.
Sb_2Te_3	980	21.7	2.36	27.4	1.22×10^{11}	Our work
Polycrystalline Bi_2Te_3	1064	3.03×10^{-5}	1.0004	3.85×10^{-5}	—	23
Graphene–Bi_2Te_3	980	10	—	11	—	24

NIR illumination with good stability and reproducibility. The corresponding on/off ratios (I_{light}/I_{dark}) are estimated to be 2.36, 3.77 and 4.23 for 1, 0.1 and 0.01 V, respectively. Furthermore, by using formulas (1) and (2), the responsivity and photoconductive gain are estimated to be 21.7, 2.31, and 0.263 A W^{-1} and 27.4, 2.93 and 0.333, for 1, 0.1 and 0.01 V, respectively. Based on these results, it can be concluded that both responsivity and gain of the device increase with increasing bias voltage. Besides, to determine how a weak irradiation could be distinguished from noise, the specific detectivity (D^*) is calculated using the following equation:[34–36]

$$D^* = \frac{RS^{1/2}}{(2qI_d)^{1/2}} = \frac{\Delta I S^{1/2}}{P_{opt}(2qI_d)^{1/2}} \quad (3)$$

where R is the responsivity, S is the effective area between the parallel electrodes, q is the electronic charge, and I_d is the dark current. By using the experimental data mentioned above, the detectivity is determined to be 1.22×10^{11}, 5.66×10^{10} and 2.07×10^{10} Jones, for 1, 0.1 and 0.01 V, respectively. In order to estimate the response speed (the time required to increase the photocurrent from 10 to 90% of the peak value or *vice versa* is defined as the rise time or the fall time, respectively) of the device, one cycle of the photoresponse of the device is plotted in Fig. 5(c), from which rise/fall times of 238.7 and 203.5 s were obtained. This response rate is much slower than that reported for other semiconductor based photodetectors. Such a slow response speed is either due to the thermo effect under NIR illumination, or the surface states (*e.g.*, surface dangling bonds and absorbents) that might act as trapping centers, leading to a reduced response speed. Table 1 summarizes the responsivity, on/off ratio, photoconductive gain and detectivity of the present device and other devices based on topological insulators. Remarkably, the main parameters of our photodetector are much better than not only the photodetector based on a polycrystalline Bi_2Te_3 film,[23] but also the graphene/Bi_2Te_3 nano-heterojunction device. The relatively good device performance can be ascribed to the location of the Dirac point near the Fermi level for the Sb_2Te_3 film.[26,37] In addition, the superior optoelectronic properties of Sb_2Te_3 film compared with that of Bi_2Te_3 are equally important reasons. Such results suggest great potential of our topological insulator photodetector for future optoelectronic device applications.

The observed high sensitivity can be attributed to the unique working mechanism, which is totally different from that of conventional semiconductor material based devices. For the present NIR photodetector, when irradiated by 980 nm illumination, the resultant photocurrent mainly consists of two parts: (1) the first contributory factor is associated with the photoconductivity effect of the bulk. Due to the relatively small bandgap of the bulk ($\sim$0.26 eV),[6] photocurrent can be easily formed as a result of generation of electron–hole pairs by photons with an energy (1.27 eV) much larger than the bandgap. Thus, the bulk contribution may dominate the photoresponse properties. (2) The second factor accounting for the photosensitivity is related to the surface states. The pure spin currents, which are a net flow of spin without a net flow of charge, are expected to propagate along the surfaces of a topological insulator in equilibrium. When illuminated with polarized light, these pure spin currents can be transformed into a spin-polarized net electrical (Fig. 6), which means out of equilibrium for the surface state.[17,38]

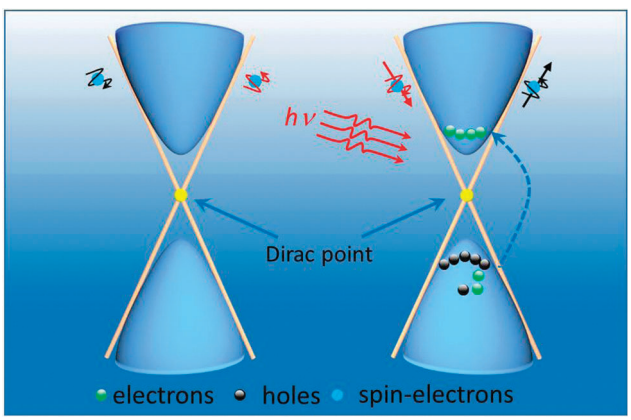

Fig. 6 Energy band diagram of the topological insulator photodetector without and with NIR light illumination.

Conclusion

In summary, we report on a NIR photodetector based on a topological insulator Sb_2Te_3 thin film which was fabricated by a MBE method. The as-fabricated NIR photodetector exhibits obvious response to NIR light, with good stability and reproducibility. Further analysis reveals that device performance of the present device in terms of responsivity, on/off ratio, photoconductive gain and detectivity are much better than that of other topological insulator material based devices. This study suggests that the current topological insulator Sb_2Te_3 device may have potential applications in future optoelectronic devices.

Experimental section

Synthesis and characterization of the topological insulator Sb_2Te_3 film

The topological insulator Sb_2Te_3 film was grown on a sapphire substrate using the MBE system under UHV conditions. The base pressure was better than 10^{-10} Torr. Both Sb (99.999%) and Te (99.999%) were evaporated from standard Knudsen cells.

The growth temperature and Sb/Te flux ratio were kept at 250 °C and 2 : 20, respectively. After synthesis, the microstructure of the Sb_2Te_3 thin film was studied by X-ray diffraction (XRD) and reflected high energy electron diffraction (RHEED). In addition, angle-resolved photoemission spectroscopy (ARPES) analysis was carried out to study the electronic properties of the Sb_2Te_3 film.

Device construction and analysis

Since the topological insulator Sb_2Te_3 film is sensitive to acetone, which is usually used to remove the photoresist during the photolithography process, a shadow mask instead of photolithography was employed to define the metal electrode during the fabrication of the NIR photodetector. Briefly, a copper foil shadow mask was placed on the surface of the topological insulator of the Sb_2Te_3 thin film, followed by deposition of 25 nm titanium and 35 nm gold films by high vacuum electron beam evaporation. Finally, a drop of silver paste was glued to the Ti/Au electrode. The device characteristics of the topological insulator Sb_2Te_3 film were measured using a semiconductor characterization system (Keithley 4200-SCS), equipped with an automatic cooling system (CCS-350 slow temperature cycle refrigeration system). During the optoelectronic study, a 980 nm laser was employed to provide monochromatic light, which was directly guided to the NIR device.

Acknowledgements

This work was supported by the Natural Science Foundation of China (NSFC, No. 61106010, 21101051), the Fundamental Research Funds for the Central Universities (2011HGZJ0004, 2012HGCX0003, 2013HGCH0012, and 2014HGCH0005), and the Ministry of Science and Technology of Taiwan (NSC, 103-2923-M-006-001).

References

1 S. K. Jerng, K. Joo, Y. Kim, S. M. Yoon, J. H. Lee, M. Kim, J. S. Kim, E. Yoon, S. H. Chun and Y. S. Kim, *Nanoscale*, 2013, **5**, 10618–10622.
2 T. Zhang, P. Cheng, X. Chen, J. F. Jia, X. Ma, K. He, L. Wang, H. Zhang, X. Dai, Z. Fang, X. Xie and Q. K. Xue, *Phys. Rev. Lett.*, 2009, **103**, 266803.
3 G. Wang, X. Zhu, J. Wen, X. Chen, K. He, L. Wang, X. Ma, Y. Liu, X. Dai, Z. Fang, J. Jia and Q. Xue, *Nano Res.*, 2010, **3**, 874–880.
4 H. B. Zhang, H. Li, J. M. Shao, S. W. Li, D. H. Bao and G. W. Yang, *ACS Appl. Mater. Interfaces*, 2013, **5**, 11503–11508.
5 Y. Tanaka, Z. Ren, T. Sato, K. Nakayama, S. Souma, T. Takahashi, K. Segawa and Y. Ando, *Nat. Phys.*, 2012, **8**, 800–803.
6 G. Bendt, S. Zastrow, K. Nielsch, P. S. Mandal, J. S. Barriga, O. Rader and S. Schulz, *J. Mater. Chem. A*, 2014, **2**, 8215–8222.
7 X. Chen, X. C. Ma, K. He, J. F. Jia and Q. K. Xue, *Adv. Mater.*, 2011, **23**, 1162–1165.
8 Z. Q. Zeng, T. A. Morgan, D. S. Fan, C. Li, Y. Hirono, X. Hu, Y. F. Zhao, J. S. Lee, J. Wang, Z. M. Wang, S. Q. Yu, M. E. Hawkridge, M. Benamara and G. J. Salamo, *AIP Adv.*, 2013, **3**, 072112.
9 M. Z. Hasan and C. L. Kane, *Rev. Mod. Phys.*, 2010, **82**, 3045–3067.
10 J. E. Moore, *Nature*, 2010, **464**, 194–198.
11 J. Wang, A. M. Dasilva, C. Z. Chang, K. He, J. K. Jain, N. Samarth, X. C. Ma, Q. K. Xue and M. H. W. Chan, *Phys. Rev. B: Condens. Matter Mater. Phys.*, 2011, **83**, 245438.
12 Y. Xia, D. Qian, D. Hsieh, L. Wray, A. Pal, H. Lin, A. Bansil, D. Grauer, Y. S. Hor, R. J. Cava and M. Z. Hasan, *Nat. Phys.*, 2009, **5**, 398–402.
13 Y. H. Wang, D. Hsieh, D. Pilon, L. Fu, D. R. Gardner, Y. S. Lee and N. Gedik, *Phys. Rev. Lett.*, 2011, **107**, 207602.
14 A. Kitaev and J. Preskill, *Phys. Rev. Lett.*, 2006, **96**, 110404.
15 G. P. Collins, *Sci. Adv. Mater.*, 2006, **294**, 56–63.
16 D. Pesin and A. H. Macdonald, *Nat. Mater.*, 2012, **11**, 409–416.
17 J. W. McIver, D. Hsieh, H. Steinberg, P. J. Herrero and N. Gedik, *Nat. Nanotechnol.*, 2012, **7**, 96–100.
18 A. Junck, G. Refael and F. von Oppen, *Phys. Rev. B: Condens. Matter Mater. Phys.*, 2013, **88**, 075144.
19 C. Zang, X. Qi, L. Ren, G. L. Hao, Y. D. Liu, J. Li and J. X. Zhong, *Appl. Surf. Sci.*, 2014, **316**, 341–347.
20 X. L. Qi and S. C. Zhang, *Rev. Mod. Phys.*, 2011, **83**, 1057–1110.
21 J. M. Shao, H. Li and G. W. Yang, *Nanoscale*, 2014, **6**, 3513–3517.
22 Y. Q. Yu, L. B. Luo, M. Z. Wang, B. Wang, L. H. Zeng, C. Y. Wu, J. S. Jie, J. W. Liu, L. Wang and S. H. Yu, *Nano Res.*, 2015, **8**, 1098–1107.
23 H. B. Zhang, J. D. Yao, J. M. Shao, H. Li, S. W. Li, D. H. Bao, C. X. Wang and G. W. Yang, *Sci. Rep.*, 2014, **4**, 5678.
24 H. Qiao, J. Yuan, Z. Q. Xu, C. Y. Chen, S. H. Lin, Y. S. Wang, J. C. Song, Y. Liu, Q. Khan, H. Y. Hoh, C. X. Pan, S. J. Li and Q. L. Bao, *ACS Nano*, 2015, **9**, 1886–1894.
25 H. B. Zhang, H. L. Yu and G. W. Yang, *Europhys. Lett.*, 2011, **95**, 56002.
26 H. J. Zhang, C. X. Liu, X. L. Qi, X. Dai, Z. Fang and S. C. Zhang, *Nat. Phys.*, 2009, **5**, 438–442.
27 H. W. Liu, H. T. Yuan, N. Fukui, L. Zhang, J. F. Jia, Y. Iwasa, M. W. Chen, T. Hashizume, T. Sakurai and Q. K. Xue, *Cryst. Growth Des.*, 2010, **10**, 4491–4493.
28 M. Z. Wang, W. J. Xie, H. Hu, Y. Q. Yu, C. Y. Wu, L. Wang and L. B. Luo, *Appl. Phys. Lett.*, 2013, **103**, 213111.
29 L. B. Luo, J. J. Chen, M. Z. Wang, H. Hu, C. Y. Wu, Q. Li, L. Wang, J. A. Huang and F. X. Liang, *Adv. Funct. Mater.*, 2014, **24**, 2794–2800.
30 C. Yang, C. J. Barrelet, F. Capasso and C. M. Lieber, *Nano Lett.*, 2006, **6**, 2929–2934.
31 B. Nie, J. G. Hu, L. B. Luo, C. Xie, L. H. Zeng, P. Lv, F. Z. Li, J. S. Jie, M. Feng, C. Y. Wu, Y. Q. Yu and S. H. Yu, *Small*, 2013, **9**, 2872–2879.
32 C. Soci, A. Zhang, B. Xiang, S. A. Dayeh, D. P. R. Aplin, J. Park, X. Y. Bao, Y. H. Lo and D. Wang, *Nano Lett.*, 2007, **7**, 1003–1009.

33 L. B. Luo, F. X. Liang and J. S. Jie, *Nanotechnology*, 2011, **22**, 485701.
34 X. Gong, M. H. Tong, Y. J. Xia, W. Z. Cai, J. S. Moon, Y. Cao, G. Yu, C. L. Shieh, B. Nilsson and A. J. Heeger, *Science*, 2009, **325**, 1665–1667.
35 L. H. Zeng, M. Z. Wang, H. Hu, B. Nie, Y. Q. Yu, C. Y. Wu, L. Wang, J. G. Hu, C. Xie, F. X. Liang and L. B. Luo, *ACS Appl. Mater. Interfaces*, 2013, **5**, 9362–9366.
36 K. K. Manga, J. Z. Wang, M. Lin, J. Zhang, M. Nesladek, V. Nalla, W. Ji and K. P. Loh, *Adv. Mater.*, 2012, **24**, 1697–1702.
37 Y. L. Chen, J. G. Analytis, J. H. Chu, Z. K. Liu, S. K. Mo, X. L. Qi, H. J. Zhang, D. H. Lu, X. Dai, Z. Fang, S. C. Zhang, I. R. Fisher, Z. Hussain and Z. X. Shen, *Science*, 2009, **325**, 178.
38 C. Jozwiak, C. Park, K. Gotlieb, C. Hwang, D. Lee, S. G. Louie, J. D. Denlinger, C. R. Rotundu, R. J. Birgeneau, Z. Hussain and A. Lanzara, *Nat. Phys.*, 2013, **9**, 293–298.

